

Ftuy][p][ggyh



**UNIDIRECTIONAL WIDEBAND ANTENNA WITH IMPROVED
CIRCULAR PARASITIC ELEMENT FOR MICROWAVE BREAST
IMAGING APPLICATIONS**



DOCTOR OF PHILOSOPHY

2024



**Faculty of Electronics and Computer Technology and
Engineering**

**UNIDIRECTIONAL WIDEBAND ANTENNA WITH IMPROVED
CIRCULAR PARASITIC ELEMENT FOR MICROWAVE BREAST
IMAGING APPLICATIONS**

Nur ' Atika Binti Koma'rudin

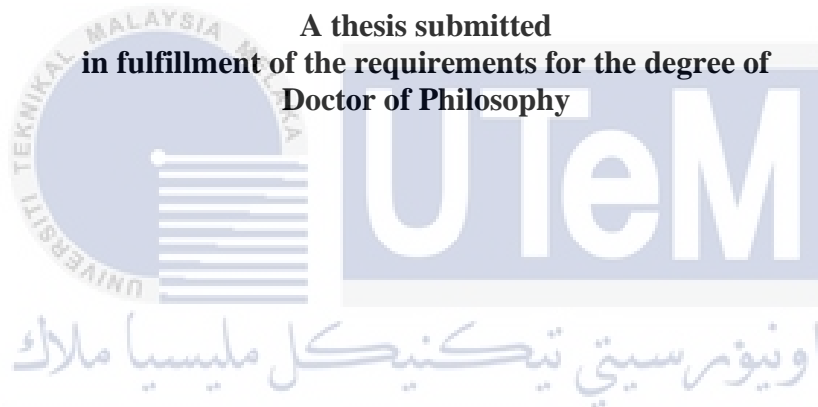
UNIVERSITI TEKNIKAL MALAYSIA MELAKA

PhD

2024

**UNIDIRECTIONAL WIDEBAND ANTENNA WITH IMPROVED CIRCULAR
PARASITIC ELEMENT FOR MICROWAVE BREAST IMAGING
APPLICATIONS**

NUR ' ATIKA BINTI KOMA'RUDIN



Faculty of Electronics and Computer Technology and Engineering

UNIVERSITI TEKNIKAL MALAYSIA MELAKA

2024

DEDICATION

Dedicated to ALLAH Almighty, my loving husband, parents and all my family's members
for your infinite and unfading love, sacrifice, best wishes, patience, and encouragement.



ABSTRACT

Early cancer detection, especially in the breast, is crucial due to its asymptomatic nature. Intricate measurement techniques are essential for accurate cancer identification, with the antenna being a key element. Ideally, it should be flexible, unidirectional, wideband, lightweight, and compact compared to previous research, improving antenna performance for precise measurements in breast cancer detection using a radar-based approach. The research aims to create a unidirectional, interference-avoiding, wideband antenna using flexible material. It presents a co-planar waveguide (CPW) wideband antenna with felt material for the 3 GHz to 7 GHz frequency range, incorporating a double-layer reflector for enhanced unidirectionality and flexibility. To confirm the antenna's performance, a model of a breast (breast phantom) was created and assessed, achieving a safe SAR level below 1.65 W/kg at a 10 mm distance. In microwave breast cancer detection, strict limitations on antenna size exist to accommodate the limited breast area, requiring a maximum typical diameter for unidirectional radiation and signal distortion suppression. The proposed antenna, enhanced by a double-reflector element, exhibited improved performance, broad 3.06 GHz to 7.0 GHz bandwidth, with measurement result of directivity (6.98 dBi), FBR (9.81 dB), and gain (5.44 dBi). The antenna and breast phantom, connected to a vector network analyzer, utilized a MATLAB algorithm (modified Delay and Sum imaging) for signal processing and image reconstruction. They successfully detected five different sizes of breast cancer with outstanding measurement responses, including cancers as small as 1 millimeter, consistent with simulation results.

اونيورسيتي تيكنيكل مليسيا ملاك

UNIVERSITI TEKNIKAL MALAYSIA MELAKA

**ANTENA JALUR LEBAR EKAARAH DENGAN ELEMEN PARASITIK BULAT
YANG DIPERTINGKAT UNTUK APLIKASI PENGIMEJAN PAYUDARA
MENGUNAKAN GELOMBANG MIKRO**

ABSTRAK

Penemuan kanser awal, terutamanya dalam payudara, adalah penting disebabkan sifatnya yang tidak menunjukkan gejala. Teknik pengukuran yang rumit adalah penting untuk pengenalpastian kanser yang tepat, dengan penggunaan antena sebagai kunci utama. Idealnya, antena seharusnya mudah lentur, satu arah, berjalur lebar, ringan, dan kecil berbanding dengan penyelidikan terdahulu, dapat meningkatkan prestasi antena untuk pengukuran yang tepat dalam pengesanan kanser payudara menggunakan pendekatan berdasarkan radar. Kajian ini bertujuan untuk mencipta antena satu arah, mengelakkan gangguan interfeferens, berjalur lebar dengan menggunakan bahan mudah lentur. Ia mempersembahkan antena jalur lebar pandu gelombang co-planar (CPW) untuk julat frekuensi 3 GHz hingga 7 GHz, digabungkan dengan lapisan dua elemen pemantul untuk meningkatkan antena satu arah dan kelenturan. Untuk mengesahkan prestasi antena, model payudara (phantom payudara) dicipta dan dinilai, mencapai tahap SAR selamat di bawah 1.65 W/kg pada jarak 10 mm. Dalam pengesanan kanser payudara menggunakan gelombang mikro, terdapat batasan ketat pada saiz antena untuk menyesuaikan kawasan payudara yang terhad, memerlukan diameter tipikal maksimum untuk radiasi satu arah dan mengelakkan gangguan interfeferens. Antena yang dicadangkan, ditingkatkan oleh elemen pemantul berganda, menunjukkan prestasi yang lebih baik, mempunyai julat frekuensi 3.06 GHz hingga 7.0 GHz yang luas, dengan keputusan pengukuran di mana pengarahannya (6.98 dBi), FBR (9.81 dB), dan gandaan (5.44 dBi). Antena dan phantom payudara, yang disambungkan ke analisis rangkaian vektor, menggunakan algoritma MATLAB (pemprosesan isyarat Tangguh dan Jumlah yang diubahsuai) untuk pemprosesan isyarat dan pembinaan imej. Ia berjaya mengesan lima saiz kanser payudara yang berbeza dengan respon pengukuran yang cemerlang, termasuk kanser sekecil 1 milimeter, sejajar dengan hasil simulasi.

ACKNOWLEDGEMENT

In the Name of Allah, Most Merciful, Most Gracious,

Above all, I express my gratitude to ALLAH for granting me the strength and courage to complete this thesis, bestowing the opportunity, courage, and patience for this endeavor. I feel honored to glorify His name through this small achievement.

Seeking His mercy, favor, and forgiveness, I extend my deepest thanks to my Supervisor, Professor Dr. Zahriladha Bin Zakaria, from Universiti Teknikal Malaysia Melaka (UTeM) and Associate Professor Dr. Soh Ping Jack from the University of Oulu, Finland, for their unwavering support, patience, and insightful guidance throughout this project. Special appreciation also goes to the laboratory technician for their valuable support and cooperation.

Finally, I want to express my heartfelt gratitude to my wonderful husband, Mohd Faizal Bin Mastor, my parents, kids, and family for their unwavering love and support during challenging times. Special thanks to friends, especially Dr. Nornikman Bin Hassan and Dr. Herwansyah Bin Lago, for valuable insights that enhanced my thesis. I appreciate everyone else for their friendship, assistance, and countless support. May Allah S.W.T. bless them all for their kindness and support.

TABLE OF CONTENTS

	PAGES
DECLARATION	
APPROVAL	
DEDICATION	
ABSTRACT	i
ABSTRAK	ii
ACKNOWLEDGEMENT	iii
TABLE OF CONTENTS	iv
LIST OF TABLES	vi
LIST OF FIGURES	vii
LIST OF ABBREVIATIONS	xiv
LIST OF SYMBOLS	xvi
LIST OF APPENDICES	xvii
LIST OF PUBLICATIONS	xviii
CHAPTER	
1. INTRODUCTION	1
1.1 Background	1
1.2 Problem Statement	5
1.3 Objective	8
1.4 Scope of Work	8
1.5 Research Contribution	9
1.6 Organization of Thesis	11
2. LITERATURE REVIEW	13
2.1 Introduction	13
2.2 Breast Cancer Management	13
2.3 Microwave Imaging (MWI) System	15
2.3.1 Radar- Based Approach (RBA) in Microwave Imaging	17
2.3.2 Microwave Imaging: Frequency and Resolution	23
2.4 Antenna and its Performance	25
2.4.1 Microstrip Antenna	26
2.4.2 Antenna Reciprocity and Backscattered Properties	29
2.4.3 Transmission Line (TL) Model	30
2.4.4 Rectangular and Circular Microstrip Antenna	32
2.4.5 Antenna Performance	34
2.5 Radiator Requirements of Microwave Breast Imaging (MWI) System	39
2.5.1 Wideband and Unidirectional Antenna	40
2.5.2 State of The Art on Recent Wideband and Unidirectional antenna	47
2.6 Dielectric Properties of Biological Tissues	71
2.6.1 Measurement Techniques for Dielectric Properties of Materials	71
2.6.2 Contrast between Normal and Cancer Tissues	74
2.6.3 Safety Assessment of Microwave Imaging	81
2.7 Anatomy and Phantom Modelling of Human Breast	83

2.8	Microwave Imaging Algorithm for Image Processing	86
2.9	Summary	90
3.	METHODOLOGY	92
3.1	Introduction	92
3.2	Antenna Specification	96
3.3	Design and Simulation Setup	101
3.4	Antenna Design	107
3.4.1	Antenna Design C	112
3.5	Specific Absorption Rate (SAR) Simulation	115
3.6	Hemi-sphere Breast Phantom	119
3.7	Fabrication Process	122
3.7.1	Antenna Fabrication	123
3.7.2	Breast Phantom Fabrication	126
3.8	Measurement Setup	133
3.8.1	Antenna Measurement Setup	133
3.8.2	Antenna with Breast Phantom Fabrication Setup	139
3.9	Image Reconstruction using MATLAB	142
3.10	Summary	144
4.	RESULT AND DISCUSSION	146
4.1	Introduction	146
4.2	Simulation and Measurement Result of Antenna C	155
4.3	Simulation of Specific Absorption Rate (SAR)	179
4.4	Measurement of Cancers Reconstruction using mDAS Algorithm	186
4.5	Comparison between Proposed Antenna and Related Work Result	189
4.6	Summary	191
5.	CONCLUSION	194
5.1	Conclusion	194
5.2	Suggestion for Future Work	195
	REFERENCES	198
	APPENDICES	259

LIST OF TABLES

TABLE	TITLE	PAGE
Table 2.1	Development of Radar Base Approaches (RBA)	22
Table 2.2	Imaging Frequency Implemented in Microwave imaging application	24
Table 2.3	Characteristics of four feed technique (Kumar and Ray, 2003)	43
Table 2.4	Summary on wideband and monopole antennas	67
Table 2.5	Summary of literature on dielectric contrast of malignant and normal tissue	79
Table 2.6	SAR exposure limits (Santorelli et al., 2011)	83
Table 2.7	Development of Delay-And-Sum (DAS) algorithm for image processing	90
Table 2.8	Enhancement of two research papers regarding bandwidth, directivity, FBR and gain	91
Table 3.1	Design specifications of antenna and material specification of substrate	98
Table 3.2	Dimension of the Antenna C	114
Table 3.3	Average permittivity and conductivity of several material of the layers of human body (Derneryd, et al, 1978)	120
Table 3.4	Cancer size and location used in the simulation. The surface of the glass is assumed to be $z = 0$ (mm)	122
Table 3.5	Dimension of the Antenna C (fabricated)	125
Table 3.6	Dielectric properties of the used materials at 3.0 GHz (Alshehri, 2011)	129
Table 3.7	Heterogeneous breast fatty tissue mixed materials at 3.0 GHz	131
Table 3.8	Cancer size and location used in the experiment. The surface of the glass is assumed to be $z = 0$ (mm)	133
Table 4.1	Different performance results of different second layer CPW length, L_{cpw2} of Antenna C (simulation)	149

Table 4.2	Radiation pattern of Antenna <i>C</i> at $\phi = 0^0$ and $\phi = 90^0$ different second layer CPW length, L_{cpw2} of Antenna <i>C</i>	150
Table 4.3	Surface current of Antenna <i>C</i> at $\phi = 0^0$ and $\phi = 90^0$ different second layer CPW length, L_{cpw2} of Antenna <i>C</i>	153
Table 4.4	Radiation pattern of Antenna <i>B</i> at $\phi = 0^0$ and $\phi = 90^0$	158
Table 4.5	Radiation pattern of Antenna <i>C</i> at $\phi = 0^0$ and $\phi = 90^0$ different second layer CPW length, L_{cpw2} of Antenna <i>C</i>	159
Table 4.6	Radiation pattern of Antenna <i>C</i> at $\phi = 0^0$ and $\phi = 90^0$ different second layer CPW length, L_{cpw2} of Antenna <i>C</i>	164
Table 4.7	Radiation pattern of Antenna <i>C</i> at $\phi = 0^0$ and $\phi = 90^0$ circular parasitic element width, W_c of Antenna <i>C</i>	165
Table 4.8	Surface current of of Antenna <i>C</i> at $\phi = 0^0$ and $\phi = 90^0$ circular parasitic element width, W_c of Antenna <i>C</i>	168
Table 4.9	Different performance results of Antenna <i>C</i> (simulation and measurement)	172
Table 4.10	Radiation pattern of Antenna <i>C</i> at $\phi = 0^0$ and $\phi = 90^0$	174
Table 4.11	Radiation pattern of Antenna <i>C</i> at $\phi = 0^0$ and $\phi = 90^0$ (simulation and measurement)	175
Table 4.12	Surface current of Antenna <i>C</i> at $\phi = 0^0$ and $\phi = 90^0$	177
Table 4.13	Return loss of the proposed antenna with different distance of human skin structure	181
Table 4.14	SAR simulation of the antenna with different distance	186
Table 4.15	The size and location of the cancer	189
Table 4.16	Comparison of wideband monopole antenna for breast cancer detection	190
Table 4.17	Contribution of the research	192

LIST OF FIGURES

FIGURE	TITLE	PAGE
Figure 1.1	Radar – based approach in Microwave Breast Imaging System (Craddock et al., 2008)	2
Figure 2.1	Statistic of Overall cancer patient by service for 2019 to 2020 (National Cancer Institute, 2020)	14
Figure 2.2	Top Underlying Cause of Death in Malaysia (National Cancer Institute, 2020)	15
Figure 2.3	Methodology block diagram of cancer cell detection by microwave imaging System (Fallahpour, 2013)	15
Figure 2.4	Block diagram showing the different modalities that explored for microwave-based breast cancer detection	16
Figure 2.5	Antenna as a transition device	26
Figure 2.6	Basic of Microstrip Patch antenna (Balanis 2016)	27
Figure 2.7	Return loss vs frequency whereas return loss is -38.66 dB at resonance frequency is 5.2 GHz	36
Figure 2.8	The relationship between the E-planes and H-planes	38
Figure 2.9	HPBW and FNBW in polar coordinate by (Bakshi et al., 2009)	39
Figure 2.10	Comparison of the Wideband, moderate band and narrow band response (Janine et al., 2009)	41
Figure 2.11	The topology of the projected CPW antenna based on the Locked-Key topology (Jameel et al., 2023)	48
Figure 2.12	Metamaterial-Based Frequency-Reconfigurable Textile CPW Antenna for Microwave Imaging of Breast Cancer (Hossain, et al., 2022)	49
Figure 2.13	Antenna layout with its parameters. (a) Front look, (b) Back look (Al-Ghuburi et al., 2022)	50
Figure 2.14	Proposed monopole antenna (Jan et al, 2021)	50
Figure 2.15	Geometric layout of antenna: (a) Topside view; (b) Backside view (Hossain et al., 2020)	51

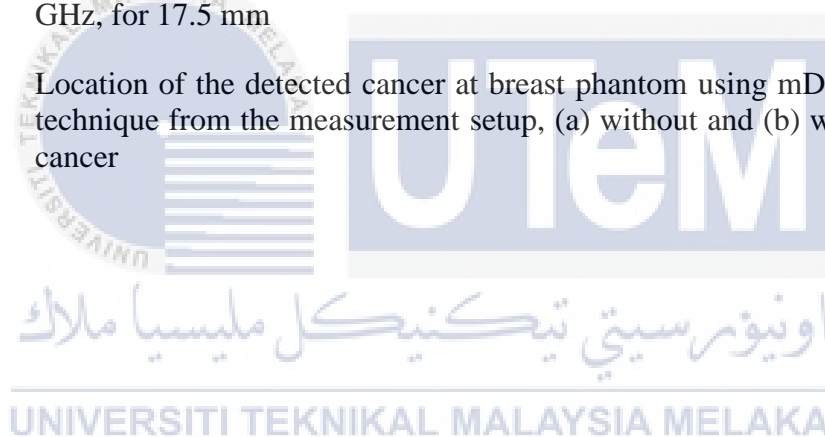
Figure 2.16	Array design of UWB fractal peano patch antenna for breast imaging on a microwave system (Ahmed et al., 2020)	52
Figure 2.17	Layout of proposed antenna (Furat et al., 2020)	53
Figure 2.18	a) Front view of the fabricated antenna, b) Back view of the fabricated antenna (Nga et al., 2020)	53
Figure 2.19	A compact Egg shaped antenna (Cherian et al., 2020)	54
Figure 2.20	Geometry of the proposed antenna, (a) top view, (b): bottom view (Fatimi et al., 2019)	55
Figure 2.21	Proposed antenna image after fabrication (a) Upper view, (b) Bottom view (Islam et al., 2019)	55
Figure 2.22	Fundamental geometry (a) exponentially tapered slot (b) proposed modified antenna (c) front view of fabricated prototype (d) back view of fabricated prototype (Islam et al., 2019)	56
Figure 2.23	UWB rectangular slot patch antenna with the full ground plane (Rahayu et al., 2019)	57
Figure 2.24	The proposed antenna (a): Front view (radiator), (b): Back view (ground plane) (Amdaouch et al., 2018)	58
Figure 2.25	Antenna structure. (a) Side view of the stacked circular patch structure. (b) 3D view showing the liquid metal tuning element and microfluidic channel in the PMMA cylinder holding the liquid metal (Xu et al., 2018)	58
Figure 2.26	Modified rectangular radiator with modified ground plane (Hammouch et al., 2018)	59
Figure 2.27	Unidirectional UWB antenna schematic: (a) front view, (b) 3D (Edalati et al., 2017)	60
Figure 2.28	The front view of the antenna using fractal technique with connector (Wang et al., 2017)	61
Figure 2.29	The proposed antenna (a), Geometric Layout b) Front Side (radiating fins), (c) Back side (Islam et al., 2017)	62
Figure 2.30	Geometry shape of the antenna by Afyf et al., 2017	62
Figure 2.31	The proposed antenna with 4-unit cells on radiation patch. (Afifi et al., 2016)	63

Figure 2.32	The design of single and dual-polarisation antennas for breast cancer detection (Bahrani et al., 2015)	64
Figure 2.33	Side view geometry of the double-ridged horn antenna designed for breast microwave imaging system (Latif et al., 2015)	65
Figure 2.34	A semicircular microstrip antenna with slotted on the patch (Gosh et al., 2014)	65
Figure 2.35	An elliptical monopole antenna with reflector on the other side (Latif et al., 2014)	66
Figure 2.36	Cavity backed aperture stacked patch antenna for breast imaging: (a) front side and (b) back side (Klemm et al., 2009)	67
Figure 2.37	Measuring dielectric properties with free space technique (Alabaster et al., 2004)	72
Figure 2.38	Measuring dielectric properties with resonant technique (Alabaster et al., 2004)	73
Figure 2.39	Measuring dielectric properties with Waveguide technique (Alabaster et al., 2004)	73
Figure 2.40	Measuring dielectric properties with Coaxial probe technique (Alabaster et al., 2004)	74
Figure 2.41	Breast Structures (Hipwell, 2014)	84
Figure 2.42	Breast Phantom Modelling (a) breast consists of four important element; skin, glandular, fat and muscle (Bahrani et al., 2015) (b) proposed breast consists of two important element; skin and fat (Alshehri et al., 2011)	85
Figure 3.1	Flow chart of the research development	94
Figure 3.2	Flow chart of the simulation setting for the antenna in CST	102
Figure 3.3	The material library in the CST Microwave Studio simulation software	103
Figure 3.4	The new material is created in the material library of CST	104
Figure 3.5	Antenna setup in CST Microwave Studio, (a) perspective view, (b) SMA port condition with coaxial waveguide port, (c) Side view of SMA connector with port	105
Figure 3.6	Boundaries setup in CST Microwave Studio	106

Figure 3.7	Flow chart of the simulation for the antenna in CST	107
Figure 3.8	Flow chart of the simulation for the antenna in CST	109
Figure 3.9	The antenna stage and development	111
Figure 3.10	Schematic diagram of front view shape and side view for Antenna A, (a) Antenna A1, (b) Antenna A2, (c) Antenna A3	113
Figure 3.11	Schematic diagram of front view shape and side view for Antenna B, (a) Antenna B1, (b) Antenna B2	117
Figure 3.12	Front view of the pentagonal Antenna C (a) first layer (b) second layer, (c) ground plane with side view	120
Figure 3.13	Cancerous breast phantom is available materials such as skin, fat and cancer	121
Figure 3.14	Cancer with different size and location used in the experiment	122
Figure 3.15	Flow chart of the antenna fabrication	123
Figure 3.16	Cutting-plotting process, (a) transparent film that printed with the proposed antenna design, (b) Cut ShieldIT based on the transparent film dimension	124
Figure 3.17	Fabrication version work of Antenna C, (a) Front view and (b) second layer view	125
Figure 3.18	SMA connector with conductive epoxy (a) using 8331 silver conductive epoxy adhesive, (b) female SMA Connectors	126
Figure 3.19	Phantom breast model setup with proposed antenna development	127
Figure 3.20	Flow chart on phantom breast development	128
Figure 3.21	The ingredient for phantom breast	130
Figure 3.22	Mixture contains petroleum jelly, flour, water and soy oil mixture of the breast phantom	131
Figure 3.23	Mixture of the phantom breast in a glass, (a) Location of cancer before insertion into breast phantom, (b) Breast phantom with a cancer inside	132
Figure 3.24	Flow chart on antenna measurement in the laboratory	134
Figure 3.25	Setup for the return loss, S_{11} measurement process	135

Figure 3.26	The IAFMS in the laboratory, (a) network analyzer and controller and (b) anechoic chamber with AUT	137
Figure 3.27	Gain measurement process in laboratory	138
Figure 3.28	Flow chart on breast phantom with the antenna measurement in the microwave laboratory	140
Figure 3.29	(a) Antenna with breast phantom measurement setup, (b) Schematic diagram	141
Figure 3.30	Flow chart on development of microwave image in MATLAB	143
Figure 4.1	Parametric study on different second layer CPW length, L_{cpw2} (a) second layer Antenna C, (b) Return Loss and frequency different second layer CPW length, L_{cpw2}	148
Figure 4.2	Different gap dimension between patch and CPW of Antenna C L_{cpw2} (a) second layer Antenna C, (b) Return Loss and frequency different gap dimension between patch and CPW of Antenna C L_{cpw2}	157
Figure 4.3	Parametric study on different circular parasitic element width, W_c of Antenna C (a) second layer Antenna C, (b) Return Loss and frequency different gap dimension circular parasitic element width, W_c of Antenna C	163
Figure 4.4	Return loss of Antenna C (Simulation and measurement)	172
Figure 4.5	Gain over frequency of Antenna C (simulation and measurement)	173
Figure 4.6	Impedance matching for resonant frequencies at 3.07 GHz and 5.15 GHz	176
Figure 4.7	Current distribution for Antenna A2 at different phase for resonant frequency of (a) 3.07 GHz at $\Phi = 0^\circ$, (b) 3.07 GHz at $\Phi = 90^\circ$, (c) 5.15 GHz @ $\Phi = 0^\circ$, (d) 5.15 GHz @ $\Phi = 90^\circ$	178
Figure 4.8	Current distribution for Antenna C at different phase for resonant frequency of (a) 3.07 GHz at $\Phi = 0^\circ$, (b) 3.07 GHz at $\Phi = 90^\circ$, (c) 5.15 GHz at $\Phi = 0^\circ$, (d) 5.15 GHz at $\Phi = 90^\circ$	179
Figure 4.9	The simulation setup for the SAR with human skin structure and the proposed antenna, (a) side view, (b) perspective view	180
Figure 4.10	Return loss of the proposed antenna with different distance of human skin structure	180

Figure 4.11	Maximum SAR of the proposed antenna with different distance of human skin structure at 3.08 GHz, 3.88 GHz, 4.42 GHz, 5.13 GHz, for 5.0 mm	182
Figure 4.12	Maximum SAR of the proposed antenna with different distance of human skin structure at 3.08 GHz, 3.88 GHz, 4.42 GHz, 5.13 GHz, for 7.5 mm	183
Figure 4.13	Maximum SAR of the proposed antenna with different distance of human skin structure at 3.08 GHz, 3.88 GHz, 4.42 GHz, 5.13 GHz, for 10.0 mm	183
Figure 4.14	Maximum SAR of the proposed antenna with different distance of human skin structure at 3.08 GHz, 3.88 GHz, 4.42 GHz, 5.13 GHz, for 12.5 mm	184
Figure 4.15	Maximum SAR of the proposed antenna with different distance of human skin structure at 3.08 GHz, 3.88 GHz, 4.42 GHz, 5.13 GHz, for 17.5 mm	184
Figure 4.16	Location of the detected cancer at breast phantom using mDAS technique from the measurement setup, (a) without and (b) with cancer	188



LIST OF ABBREVIATIONS

CMI	-	Confocal Microwave Imaging
CPW	-	Coplanar waveguide
CST	-	Computer Simulation Technology
DAS	-	Delay-and-Sum imaging
DMAS	-	Delay Multiply and Sum
EDAS	-	Enhanced Delay and Sum
EM	-	Electromagnetic
FBW	-	Voltage Standing Wave Ratio
GPR	-	Ground Penetrating Radar
IDAS	-	Improved Delay and Sum
IoT	-	Internet of Things
LHM	-	Left-Handed Metamaterial
mDAS	-	modified Delay and Sum Imaging Algorithm
MRI	-	Magnetic Resonance Imaging
MUT	-	Material Under Test
RBA	-	Radar- Based Approach
RF	-	Radio Frequency
SAR	-	Specific Absorption Rate
SCR	-	Signal to Clutter Ratio
SNR	-	Signal-to-Noise Ratio
SSVA	-	Side Slotted Vivaldi Antenna

OUT	-	Object Under Test
VNA	-	Vector Network Analyser
WB	-	Wideband
WBAN	-	Wireless Body Area Network
WLAN	-	Wireless Local Area Network



LIST OF SYMBOLS

$\tan\delta$	-	Tangent loss
ϵ_r	-	Dielectric constant
λ	-	wavelength



LIST OF APPENDICES

APPENDIX	TITLE	PAGE
Appendix A	Current Technologies of Breast Cancer Imaging	259
Appendix B	Parametric Studies of Antenna Design	269
Appendix C	Surface Current of Antenna Design	305
Appendix D	MATLAB Codes for modified Delay and Sum Imaging Algorithm (mDAS)	321
Appendix E	ShieldIT Material	326
Appendix F	CST Introduction	327



LIST OF PUBLICATIONS

The research papers produced and published during this research are as follows:

1. N. A. Koma'rudin, Z. Zakaria, P.J. Soh, H. Lago, H. Alsariera, N. Hassan, Nornikman, 2020. A Review of Recent Microwave Breast Imaging, *International Journal on Communications Antenna and Propagation (IRECAP)*. vol.10 (4). August 2020 0.257. 10.15866/irecap.v10i4.18560.
2. N. A. Koma'rudin and Z. Zakaria and A. A. Althuwayb and Herwansyah Lago and H. Alsariera and H. Nornikman and A. J. A. Al-Gburi and P. J. Soh, 2022. Directional Wideband Wearable Antenna with Circular Parasitic Element for Microwave Imaging Applications. *Computers, Materials & Continua*, vol.72 (1). pp. 983-998.
3. Nur 'Atika Koma'rudin, Zahriladha Zakaria, Ping Jack Soh, Nornikman Hassan dan Mohd Manoj Jumidali, 2023. 'Compact Dual-Layered Wideband Wearable Monopole Antenna with Circular Parasitic Element for Breast Cancer Detection'. *2023 IEEE Symposium on Industrial Electronics & Applications*. pp. 1-6.

CHAPTER 1

INTRODUCTION

1.1 Background

In recent decades, the increasing demand, particularly in military and medical applications requiring tracking, monitoring, and screening, has led to significant advancements in microwaves and radio frequencies (Guan et al., 2018). Microwave imaging represents an innovative scientific technique that has evolved from detection and location methods (such as radar or tomography) to assess objects or structures embedded or hidden in any medium using electromagnetic waves (EM) within the frequency range of ~300 MHz to 300 GHz (Fallahpour, 2013). Two main approaches have been proposed in microwave imaging: microwave tomography, based on the scattered EM field, and the radar-based approach, utilizing short pulses transmitted towards a target with measured scattered fields, as illustrated in Figure 1.1 (Craddock et al., 2008). Most researchers have reported using the radar-based approach, employing a set of antennas to transmit low-power microwave signals into tissues. Backscattered signals are then utilized to generate microwave images, providing information on the cancer's distance from the antenna (Chandra et al., 2015; Khan et al., 2016; Bourqui et al., 2010; Zarnaghi Naghsh et al., 2018; Porte et al., 2016; Zeng et al., 2011; Gibbins et al., 2017).

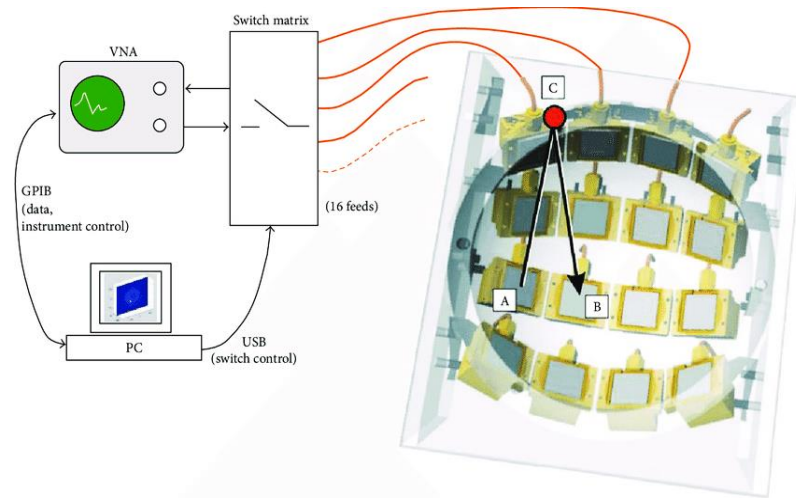


Figure 1.1: Radar – based approach in Microwave Breast Imaging System by Craddock (Craddock et al., 2008)

Due to global advancements and lifestyle changes, diseases are on the rise. In Malaysia, cancer is a significant health concern, causing 19,000 deaths per 100,000 people in 2016. It ranks third after respiratory (18.54%) and circulatory system diseases (22.77%) (my Metro, 2016; mStar, 2016). The most prevalent cancers include breast (14.5%), colorectal (12.1%), lung (11.8%), cervix (5.7%), and throat cancer (5.4%). Breast cancer tops the list for women, while lung and prostate cancer lead among men (Guan et al., 2018). Notably, 30% of breast cancers go undetected by mammography, with a high false-positive rate of around 70% in screening mammograms (Pace et al., 2014; Lazebnik et al., 2007; Chandra et al., 2015; Kwon et al., 2017).

In Malaysia, cancer detection methods often involve painful procedures. X-rays, while effective, emit ionizing radiation with potential harm. Biopsy and bronchoscopy, though accurate, can cause mental trauma. Magnetic resonance imaging (MRI) has limitations, including high costs and equipment size. Microwave imaging (MWI) emerges as a low-cost alternative, offering easy operation, high data rates, and non-invasive, non-